







RESEARCH ARTICLE | JANUARY 24 2024

Creation of color centers in diamond by recoil implantation through dielectric films

Yuyang Han ; Christian Pederson ; Bethany E. Matthews ; Nicholas S. Yama ; Maxwell F. Parsons ; Kai-Mei C. Fu 

 Check for updates

Appl. Phys. Lett. 124, 044007 (2024)

<https://doi.org/10.1063/5.0183421>

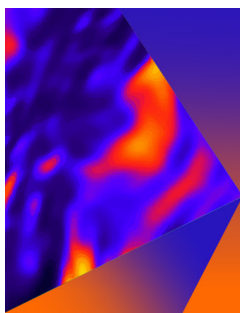


View Online



Export Citation

25 June 2024 14:59:00



Applied Physics Letters

Special Topic: Mid and Long Wavelength Infrared Photonics, Materials, and Devices

Submit Today



Creation of color centers in diamond by recoil implantation through dielectric films

Cite as: Appl. Phys. Lett. **124**, 044007 (2024); doi: [10.1063/5.0183421](https://doi.org/10.1063/5.0183421)

Submitted: 23 October 2023 · Accepted: 11 January 2024 ·

Published Online: 24 January 2024



View Online



Export Citation



CrossMark

Yuyang Han,^{1,a)} Christian Pederson,² Bethany E. Matthews,³ Nicholas S. Yama,¹ Maxwell F. Parsons,¹ and Kai-Mei C. Fu^{1,2,3}

AFFILIATIONS

¹Department of Electrical and Computer Engineering, University of Washington, Seattle, Washington 98195, USA

²Department of Physics, University of Washington, Seattle, Washington 98195, USA

³Pacific Northwest National Laboratory, Richland, Washington 99352, USA

^{a)} Author to whom correspondence should be addressed: yh236@uw.edu

ABSTRACT

The need of near-surface color centers in diamond for quantum technologies motivates the controlled doping of specific extrinsic impurities into the crystal lattice. Recent experiments have shown that this can be achieved by momentum transfer from a surface precursor via ion implantation, an approach known as “recoil implantation.” Here, we extend this technique to incorporate dielectric precursors for creating nitrogen-vacancy (NV) and silicon-vacancy (SiV) centers in diamond. Specifically, we demonstrate that gallium focused-ion-beam exposure to a thin layer of silicon nitride or silicon dioxide on the diamond surface results in the introduction of both extrinsic impurities and carbon vacancies. These defects subsequently give rise to near-surface NV and SiV centers with desirable properties after annealing.

Published under an exclusive license by AIP Publishing. <https://doi.org/10.1063/5.0183421>

In the past two decades, color centers in diamond have gained significant attention as atomic-scale sensors^{1–3} and as qubits for quantum information processing.^{4–8} The negatively charged nitrogen-vacancy (NV[−]) center is particularly attractive for sensing due to its high internal quantum efficiency,⁹ room-temperature spin initialization,¹⁰ spin readout,¹¹ and long spin coherence time. The negatively charged silicon-vacancy (SiV[−]) center shows promise for quantum network applications due to its stable, uniform, and strong optical transitions^{12,13} that are further protected from the electric field noise by its inversion symmetry.¹⁴ However, the SiV[−] center also has drawbacks such as lower quantum efficiency and shorter spin coherence time.¹⁵ Consequently, researchers are exploring alternative color centers in diamond such as other group IV defects, including germanium-vacancy (GeV), tin-vacancy (SnV), and lead-vacancy (PbV) centers.^{16–18} To better study and engineer diamond defects for quantum technologies, means of controllably creating color centers in diamonds are of great interest. Particularly, the formation of very near-surface defects (i.e., <10 nm) is desirable for their potential applications in nanoscale sensing¹⁹ and near-field photonics device coupling²⁰ for ultrafast single photon sources.²¹

The creation of these vacancy defect complexes (i.e., X–V centers) requires the presence of the extrinsic impurity X—either unintentionally or deliberately doped—and carbon vacancies, which can be

introduced by electron, ion, or laser irradiation.^{22–24} Among the techniques to create X–V defects, X-ion implantation with post-annealing has been widely used,^{25–29} as bombarding the diamond lattice with selected ions introduces both carbon vacancies and extrinsic impurities. Subsequent high-temperature anneal (usually above 800 °C) allows vacancies to diffuse to the impurities and form X–V complexes.³⁰

During implantation, the lateral position of the ions can be controlled either by customized implantation masks or focused ion beam (FIB) direct writing;^{26,31–34} the ion depth distribution by the implantation energy; and the ion density by the implantation dose, screening layers, and ion detection systems.^{25,28,35,36} Near-surface NV centers, for example, that are 1–20 nm below the diamond surface can be created by low energy (0.4–3 keV) nitrogen ion beam implantation^{37–41} and nitrogen delta-doping.⁴² Nevertheless, challenges remain in the creation of defects with sub-30 nm accuracy and close-to-unity formation yield.⁴³ FIB implantation faces additional limitation in its ion source availability.

Recently, an alternative technique known as recoil implantation^{18,44–48} was used to address the limitation of ion sources by harnessing the momentum transfer from the ion-beam to the surface precursors, including solid-state films (silicon, germanium, tin, and lead)¹⁸ and nitrogen-based gases (N₂, NF₃, and NH₃).⁴⁴ To form

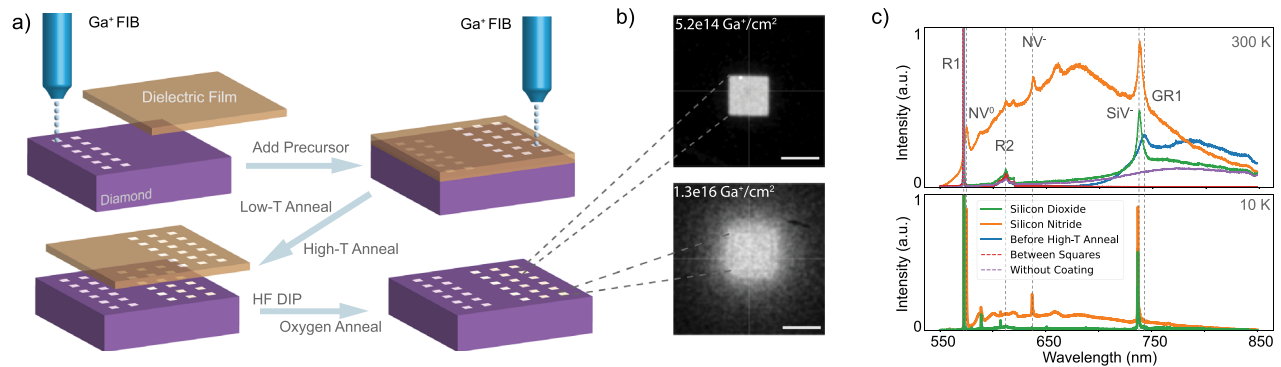


FIG. 1. Experiment overview: (a) illustration of the experiment process. The size of the implantation squares is not drawn to scale. The distance between the squares during each FIB exposure is $300\ \mu\text{m}$. (b) Representative confocal images from two of the implantation squares with different gallium fluences (P_5 for upper image and P_1 for lower image). Scale bars in the images are $10\ \mu\text{m}$. (c) Representative spectra at room temperature (upper plot) and at 10 K (lower plot). The blue line represents data obtained from a region between two squares; the purple line is taken from one of the squares irradiated with FIB prior to depositing the dielectric layers. Important wavelengths are marked by the gray dashed lines. In ascending order, these correspond to the first-order Raman line, NV^0 ZPL (575 nm), second-order Raman line, NV^- ZPL (637 nm), SiV^- ZPL (737 nm), and GR1 ZPL (741 nm).

vacancy complexes, a Xe FIB was used to displace the atoms from the surface precursors into the diamond lattice, creating both impurities and vacancies that give rise to the corresponding color centers after annealing.

In this work, we extended the recoil implantation method to the use of dielectric precursors and gallium FIB. Specifically, we implanted near-surface nitrogen and silicon atoms by employing gallium FIB implantation through a thin layer of either silicon nitride or silicon dioxide. Following high-temperature anneal and subsequent film removal, the formed NV and SiV centers displayed desirable properties. This demonstration offers a more accessible approach to generating NV centers by recoil implantation, compared to using gas-phase precursors. In general, the extension of ion-source options and precursor materials made this technique more attractive for defect engineering.

Two $2 \times 2 \times 0.5\ \text{mm}^3$ single crystal type IIa chemical-vapor-deposition (CVD) diamond samples were used as substrates. The specified nitrogen impurity concentration is less than 5 ppm (Element Six). Before the experiments, we cleaned both samples in acid and solvents (see the supplementary material). Next, a control experiment was performed on both samples to introduce lattice damage in the absence of surface precursors. Each sample was exposed to 30 keV Ga^+ ions in $12 \times 10 \times 10\ \mu\text{m}^2$ square regions. Six different FIB parameters were used for these 12 regions, with each parameter performed twice to test for variance between identical exposure conditions at different diamond surface locations [Fig. 1(a)]. The implantation parameters, from P_1 to P_6 , are summarized in Table I.

The samples were then solvent-cleaned, after which we deposited a 5 nm SiO_2 layer by electron-beam evaporation on one of the samples and a 5 nm SiN_x layer by plasma-enhanced CVD (PECVD) on the other. The deposited layers were used as surface precursors, where the same FIB exposure (Table I) was performed to create 12 new implantation squares on each sample [Fig. 1(a)]. Six additional lower-dose squares were added to the SiO_2 sample for testing a wider range of ion fluences (see the supplementary material).

The samples were cleaned in acid after the second FIB exposure; the acid clean does not strip the dielectric films⁴⁹ but removes

contaminants prior to the low-temperature anneal. This anneal, at 460°C for four hours in an O_2 atmosphere, allows the carbon self-interstitials to diffuse,⁵⁰ thus healing some of the irradiation-induced damage (see the supplementary material). However, the relatively low temperature does not lead to vacancy complex formation.⁵¹ Hence, this is followed by a high-temperature anneal at 900°C for 2 h in a vacuum environment (see the supplementary material). 25% hydrofluoric acid (HF) was used to strip both dielectric layers after annealing. Finally, an oxygen-anneal (see the supplementary material) was performed on both samples to remove the irradiation-induced sp^2 carbon and oxygen terminate the surface for charge-state conversion to NV^- .⁵²

After the low-temperature anneal and before the high-temperature anneal, PL confocal imaging and spectroscopy of all implantation squares was measured at room temperature with 532 nm excitation. Representative confocal images are displayed in Fig. 1(b), where a fluorescent square was found in each implanted region with the expected $10 \times 10\ \mu\text{m}^2$ size. An obvious halo was observed outside each of the three highest-dose squares (with FIB parameters P_1, P_2 , and P_3). This was attributed to neutralized gallium ions that were not fully focused. Spectra acquired from these fluorescent regions confirmed that the fluorescence comes from the GR1 center (neutral monovacancy defect) emission [Fig. 1(c)]. Both the PL spectrum and intensity

TABLE I. FIB parameters and estimated ion fluences: dwell time refers to how long the ion beam is at any location during one raster scan; pass represents the number of exposures performed on the same square region.

Parameter	I (nA)	Dwell (μs)	Pass	Fluence (cm^{-2})
P_1	0.79	1	10	$(1.30 \pm 0.14) \times 10^{16}$
P_2	0.79	1	2	$(2.61 \pm 0.28) \times 10^{15}$
P_3	0.43	1	1	$(1.14 \pm 0.15) \times 10^{15}$
P_4	0.08	1	1	$(9.7 \pm 2.8) \times 10^{14}$
P_5	0.024	1	1	$(5.19 \pm 0.50) \times 10^{14}$
P_6	0.0077	1	1	$(2.87 \pm 0.36) \times 10^{14}$

were consistent across the squares with identical FIB parameters, implying no intrinsic variation among different locations on the sample surface.

After the oxygen-anneal, the PL emission changed from GR1 to NV and SiV⁻. As shown in Fig. 1(c), the SiO₂ sample squares displayed a strong SiV⁻ ZPL, while the SiN_x sample squares had additional strong NV⁰ and NV⁻ ZPLs. This indicated that both the NV and SiV centers were created from the dielectric films. The control experiment confirmed that recoil implantation was the source of the doped nitrogen and silicon atoms, rather than diffusion from the dielectric films into the irradiated diamond during annealing. Additionally, a broadband irradiation-induced fluorescence was measured from all squares [Fig. 1(c), purple line].

Around the highest-fluence implantation square from each sample, we took a hyperspectral image (Fig. 2). Comparing the SiN_x sample to the SiO₂ sample, the NV ZPL in the former was notably brighter within the irradiated region, while the latter had a more homogeneous intensity distribution. This confirmed that the NV centers in the SiN_x sample arose from the nitrogen-based precursor, rather than from the naturally occurring impurities as in the SiO₂ sample.

To calculate the formation yield of the NV and SiV centers, we first simulated the nitrogen and silicon atom distribution by TRIM⁵³ and obtained the number of recoil-implanted atoms per gallium ion [Figs. 3(a) and 3(b)]. Relative contributions to the total PL intensity [Fig. 3(c)] from the different color centers were then estimated by fitting the PL spectra with a weighted sum of NV⁰ spectrum, NV⁻ spectrum, SiV⁻ spectrum, and the “irradiation-induced fluorescence” spectrum [Fig. 1(c), purple line]. After normalizing the respective PL intensity to that from a sample with the known defect density, we derived the formation yield [Fig. 3(d)] for NV and SiV centers in both samples (see the supplementary material). The maximum yield was in the order of 0.001%, much lower than 0.5%–50% that was obtained by direct ion implantation.^{25,26,28,35,54–56} However, this was expected as the implanted atoms were not only very close to the surface but also in regions of very high ion fluence. Very near-surface color centers are

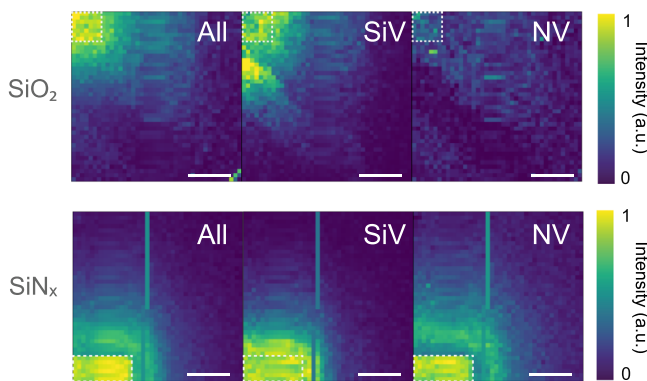


FIG. 2. Hyperspectral images of the highest-dose implantation squares from the SiO₂ sample and the SiN_x sample. The excitation power was 4.2 mW. From left to right, the intensity plots were obtained by: (All) integrating the total PL intensity over the 625–792 nm confocal bandwidth; (SiV) binning the SiV⁻ ZPL; and (NV) binning the NV⁻ ZPL. Binning was performed by fitting and integrating over the corresponding ZPL (see the supplementary material). The plots were not normalized to the same intensity. The implantation-square border was marked by the white dashed line in each plot. The scale bars in the plots were 10 μm .

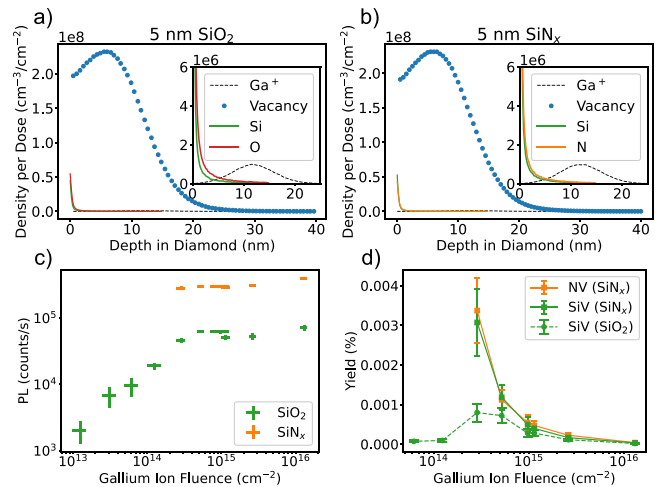


FIG. 3. Formation yield estimate: TRIM simulations of 30 keV incident Ga⁺ beam on diamond with (a) 5 nm electron-evaporation SiO₂ (2.658 g/cm³) and (b) 5 nm PECVD SiN_x (2.5 g/cm³). To derive the effective implantation dose of nitrogen and silicon atoms, integration over the simulation depth was performed, followed by multiplication with the gallium ion dose (supplementary material). This resulted in 1.83 silicon atom per gallium ion for the SiO₂ sample and 2.18 silicon plus 2.19 nitrogen atoms per gallium ion for the SiN_x sample. (c) Confocal PL intensities for all implantation squares measured at 0.2 mW 532 nm excitation. The vertical width of each data point showed the standard deviation of the measured PL intensities inside the square; the horizontal width showed the uncertainty in ion fluence. (d) Formation yield for SiV and NV centers from the SiN_x and SiO₂ samples that is computed based on (a), (b), and (c).

less fluorescent,^{37,57} and excessive ion fluence can damage the crystal lattice thus leading to low formation yield.^{26,37} Because the lattice damage increases with the ion fluence, the “saturated” PL intensities for the six highest-dose squares [Fig. 3(c)] imply that we have used excessive dose for all SiN_x squares. However, it was still possible to probe lower-dose conditions by taking measurements in the halo region, where the fluence of the neutralized gallium ions should be much lower. As shown by Fig. 3(d), the yield of the SiV centers was higher in the SiN_x sample. This is likely because the SiV²⁻ (dark state) can capture holes that are photo-generated from the nearby NV⁰ centers and become SiV⁻ (bright state).⁵⁸

To characterize the optical properties of the formed defects, we measured the PL spectra from all implantation squares at 10 K. Most SiV centers from the squares exhibited four distinct main transition peaks, whereas the NV centers showed large inhomogeneous broadening [Figs. 4(a) and 4(b)]. Among the SiV⁻ centers, we found the smallest inhomogeneous broadening (FWHM) of 16 GHz from the halo region of the highest-dose square in the SiO₂ sample. This inhomogeneous linewidth was close to the spectrometer limit (10 GHz); similar linewidths from several other implantation squares were all comparable to the 15 GHz linewidth observed in the literature by direct silicon ion implantation.⁵⁹ Nevertheless, the recoil-implanted SiV centers were 10 times closer to the diamond surface (less than 10 nm compared to around 100 nm), which typically would lead to spectral diffusion due to the unfavorable surface strain and charge environment. In particular, other implanted defects, such as the substitutional gallium, which is an acceptor,⁶⁰ and the nitrogen defect, which is a donor,⁵⁷ will

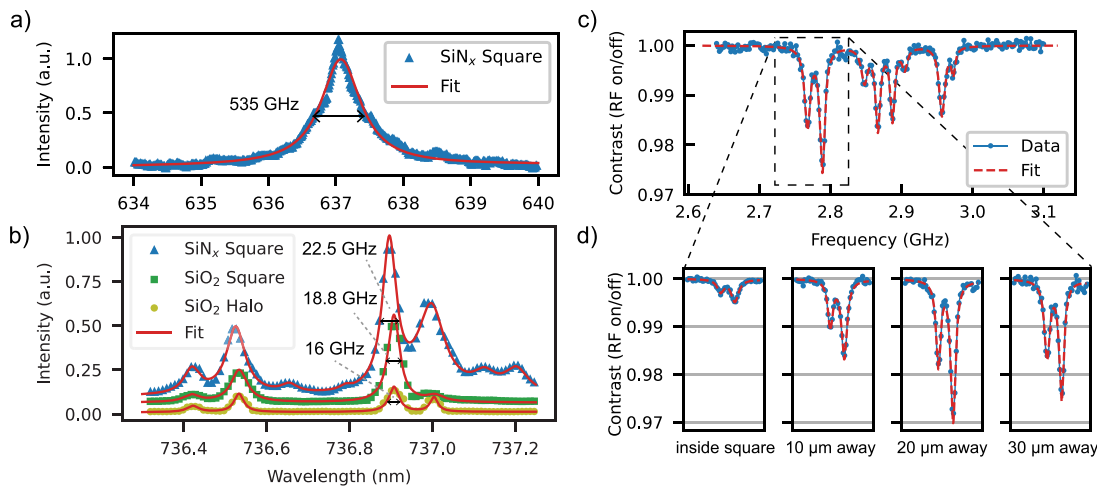


FIG. 4. Defect characterization: (a) 10 K PL spectrum of NV^- centers from the SiN_x sample. The spectrum was fit with a Lorentzian function to determine a FWHM of 535 GHz. (b) 10 K PL spectra of SiV^- center(s) from both samples. The spectrum from an implantation square on the SiN_x sample (labeled “ SiN_x square”) was fit by eight Lorentzian functions; the spectrum from a square on the SiO_2 sample (labeled “ SiO_2 square”) and the spectrum from the halo region around this square (labeled “ SiO_2 Halo”) were each fit with four Lorentzian functions. The spectra shown in (b) were scaled and shifted for better visualization. (c) Representative ODMR spectrum from NV^- centers in the halo region of highest-fluence square on the SiN_x sample. The same experiments were performed when the excitation beam was inside the square, 10, 20, and 30 μm away from the center of the square. The first two resonances from these measurements are shown in (d). The asymmetric spectrum intensity comes from the finite bandwidth of our microwave antenna (supplementary material).

affect the equilibrium and dynamic charge state of the target impurity. Charging and discharging of these nearby defects can also contribute further to fluctuations in the electrostatic environment, although in some cases more nitrogen can reduce such adverse fluctuations.⁶¹

We further investigated the spin coherence of the NV^- centers from the highest-dose square on the SiN_x sample, by conducting continuous wave optically detected magnetic resonance (CW-ODMR). In the presence of a 24 G external magnetic field, we observed four pairs of resonance dips that corresponded to the four different crystallographic orientations of NV^- centers [Fig. 4(c)]. As the excitation beam moved from inside this square to the halo region, the maximum PL contrast for a single resonance dip increased from 0.47% to 2.94%, while the average linewidth (FWHM) decreased from 10.3 to 8.37 MHz [Fig. 4(d)]. This suggested that the spin-coherence of the

NV^- centers would benefit from lower ion fluences than what we used in this study. Additionally, these linewidths were broadened by the 2 mW excitation power.⁶² We obtained the narrowest spectrum with a linewidth of 6.81 MHz using 0.1 mW excitation power (see the supplementary material). This observed 2.94% contrast was approximately half of the expected maximum. This was due to the lower NV^-/NV^0 ratio and the additional background PL from the SiV^- centers (see the supplementary material). The reduction in ODMR contrast served as a trade-off for having NV^- sensors at these shallow depths and might be improved by additional surface preparations.

Additional TRIM simulations were performed with an SiO_2 precursor to explore the flexibility provided by recoil implantation. As shown in Fig. 5, both the carbon vacancy and the silicon atom distributions can be adjusted by varying the ion energy and the SiO_2 layer

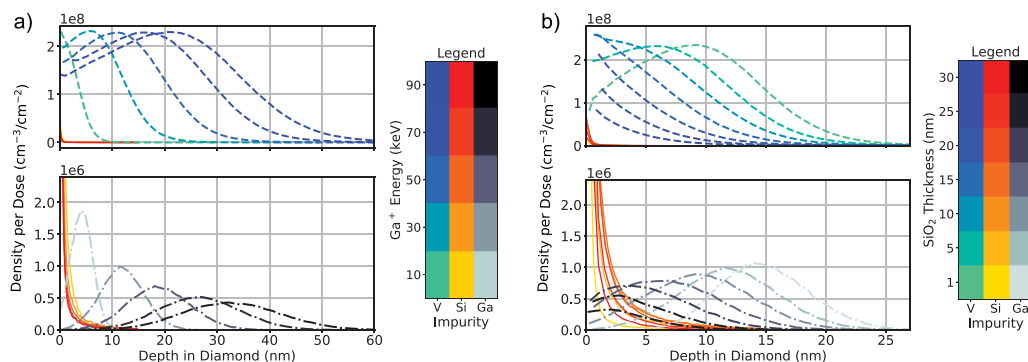


FIG. 5. TRIM simulation of recoil implantation with variable ion energy and SiO_2 thickness. (a) Impurity distribution using a 5 nm SiO_2 layer with variable ion energies. (b) Impurity distribution using 30 keV gallium ion energy with variable SiO_2 layer thickness. The horizontal axis labeled “depth in diamond (nm)” represents the depth measured from the diamond surface. The colors of the impurity distributions are represented in the legend of each plot.

thickness. This semi-independent control was not possible by direct silicon ion implantation, where the vacancy to silicon atom ratio was set by the implantation energy only. Potentially, this new degree of freedom allows for forming better defects by controlling the distribution of the gallium impurities. For example, Fig. 5(a) suggests that a large implantation energy sends the Ga^+ ions to a different depth from these silicon atoms. Alternatively, Fig. 5(b) implies that a very thin layer of SiO_2 will achieve the same effect, while additionally realizing a much smaller range of depth for the silicon atoms. This opens the possibility of forming a 2D layer of defects on the crystal surface. In this case, the lateral straggle is expected to be small, which indicates that the spatial resolution is only limited by the ion beam.

To conclude, we demonstrated gallium FIB recoil implantation through dielectric precursors for generating color centers in diamond. The use of silicon-dioxide and silicon-nitride films in this experiment expanded the range of applicable surface precursors to include dielectric materials, exemplified by the formation of near-surface SiV and NV centers. These SiV centers exhibited narrow inhomogeneous broadening that were promising for performing photoluminescence excitation and photonics device coupling, while the NV centers displayed reasonable ODMR spectra, highlighting their efficacy in quantum sensing applications. Simulations also underscored the flexibility of this technique, especially the degrees of freedom to fine-tune the spatial distributions and density profiles of the implanted atoms.

See the supplementary material for the details on experimental process, spectral fitting, formation yield calculation, inhomogeneous broadening, spin coherence, and defect localization.

This material is based upon work primarily supported by Department of Energy, Office of Science, National Quantum Information Science Research Centers, Co-design Center for Quantum Advantage (C2QA), under Contract No. DE-SC0012704, partially supported by NSF PHY-GRS 2233120. The FIB implantation was performed at the Pacific Northwest National Laboratory. The dielectric film deposition was performed at the Washington Nanofabrication Facility, a National Nanotechnology Coordinated Infrastructure (NNCI) site at the University of Washington with partial support from the National Science Foundation via Award Nos. NNCI-1542101 and NNCI-2025489. The optical and ODMR measurements were performed in the Quantum Technologies Training and Testbed (QT3) user facility, supported by the National Science Foundation under Award Nos. OMA-1936100 and OMA-1936932. The authors would like to thank Adam Cox and Chukwuemeka Mordi for their contributions in software development.

AUTHOR DECLARATIONS

Conflict of Interest

The authors have no conflicts to disclose.

Author Contributions

Yuyang Han: Conceptualization (equal); Data curation (equal); Formal analysis (equal); Investigation (equal); Writing – original draft (equal); Writing – review & editing (equal). **Christian Pederson:** Data curation (equal); Investigation (equal); Writing – review & editing

(equal). **Bethany E. Matthews:** Data curation (equal); Writing – review & editing (equal). **Nicholas S. Yama:** Data curation (equal); Writing – review & editing (equal). **Maxwell F. Parsons:** Conceptualization (equal); Data curation (equal); Formal analysis (equal); Funding acquisition (equal); Investigation (equal); Methodology (equal); Project administration (equal); Software (equal); Supervision (equal); Writing – original draft (equal); Writing – review & editing (equal). **Kai-Mei Fu:** Conceptualization (equal); Data curation (equal); Formal analysis (equal); Funding acquisition (equal); Investigation (equal); Methodology (equal); Project administration (equal); Software (equal); Supervision (equal); Writing – original draft (equal); Writing – review & editing (equal).

DATA AVAILABILITY

The data that support the findings of this study are available from the corresponding author upon reasonable request.

REFERENCES

- J. R. Maze, P. L. Stanwix, J. S. Hodges, S. Hong, J. M. Taylor, P. Cappellaro, L. Jiang, M. V. G. Dutt, E. Togan, A. S. Zibrov, A. Yacoby, R. L. Walsworth, and M. D. Lukin, “Nanoscale magnetic sensing with an individual electronic spin in diamond,” *Nature* **455**(7213), 644–647 (2008).
- J. F. Barry, M. J. Turner, J. M. Schloss, D. R. Glenn, Y. Song, M. D. Lukin, H. Park, and R. L. Walsworth, “Optical magnetic detection of single-neuron action potentials using quantum defects in diamond,” *Proc. Natl. Acad. Sci. U. S. A.* **113**(49), 14133–14138 (2016).
- G. Balasubramanian, I. Y. Chan, R. Kolesov, M. Al-Hmoud, J. Tisler, C. Shin, C. Kim, A. Wojcik, P. R. Hemmer, A. Krueger, T. Hanke, A. Leitenstorfer, R. Bratschkitsch, F. Jelezko, and J. Wrachtrup, “Nanoscale imaging magnetometry with diamond spins under ambient conditions,” *Nature* **455**(7213), 648–651 (2008).
- Y. Fu, W. Liu, X. Ye, Y. Wang, C. Zhang, C.-K. Duan, X. Rong, and J. Du, “Experimental investigation of quantum correlations in a two-qutrit spin system,” *Phys. Rev. Lett.* **129**(10), 100501 (2022).
- F. Dolde, V. Bergholm, Y. Wang, I. Jakobi, B. Naydenov, S. Pezzagna, J. Meijer, F. Jelezko, P. Neumann, T. Schulte-Herbrüggen, J. Biamonte, and J. Wrachtrup, “High-fidelity spin entanglement using optimal control,” *Nat. Commun.* **5**(1), 3371 (2014).
- H. Bernien, B. Hensen, W. Pfaff, G. Koolstra, M. S. Blok, L. Robledo, T. H. Taminiau, M. Markham, D. J. Twitchen, L. Childress, and R. Hanson, “Heralded entanglement between solid-state qubits separated by three metres,” *Nature* **497**(7447), 86–90 (2013).
- A. Delteil, Z. Sun, W.-b. Gao, E. Togan, S. Faelt, and A. Imamoglu, “Generation of heralded entanglement between distant hole spins,” *Nat. Phys.* **12**(3), 218–223 (2016).
- S. L. N. Hermans, M. Pompili, H. K. C. Beukers, S. Baier, J. Borregaard, and R. Hanson, “Qubit teleportation between non-neighbouring nodes in a quantum network,” *Nature* **605**(7911), 663–668 (2022).
- A. Mohtashami, M. Frimmer, and A. Femius Koenderink, “Quantum efficiency of single NV centers in nanodiamonds,” in *Conference on Lasers and Electro-Optics—International Quantum Electronics Conference* (Optica Publishing Group, 2013).
- V. Jacques, P. Neumann, J. Beck, M. Markham, D. Twitchen, J. Meijer, F. Kaiser, G. Balasubramanian, F. Jelezko, and J. Wrachtrup, “Dynamic polarization of single nuclear spins by optical pumping of NV color centers in diamond at room temperature,” *Phys. Rev. Lett.* **102**(5), 057403 (2009).
- L. Robledo, L. Childress, H. Bernien, B. Hensen, P. F. A. Alkemade, and R. Hanson, “High-fidelity projective read-out of a solid-state spin quantum register,” *Nature* **477**(7366), 574–578 (2011).
- L. J. Rogers, K. D. Jahnke, T. Teraji, L. Marseglia, C. Müller, B. Naydenov, H. Schaffert, C. Kranz, J. Isoya, L. P. McGuinness, and F. Jelezko, “Multiple intrinsically identical single-photon emitters in the solid state,” *Nat. Commun.* **5**(1), 4739 (2014).

- ¹³E. Neu, D. Steinmetz, J. Riedrich-Möller, S. Gsell, M. Fischer, M. Schreck, and C. Becher, "Single photon emission from silicon-vacancy colour centres in chemical vapour deposition nano-diamonds on iridium," *New J. Phys.* **13**(2), 025012 (2011).
- ¹⁴A. Sipahigil, K. D. Jahnke, L. J. Rogers, T. Teraji, J. Isoya, A. S. Zibrov, F. Jelezko, and M. D. Lukin, "Indistinguishable photons from separated silicon-vacancy centers in diamond," *Phys. Rev. Lett.* **113**(11), 113602 (2014).
- ¹⁵B. Pingault, J. N. Becker, C. H. H. Schulte, C. Arend, C. Hepp, T. Godde, A. I. Tartakovskii, M. Markham, C. Becher, and M. Atatüre, "All-optical formation of coherent dark states of silicon-vacancy spins in diamond," *Phys. Rev. Lett.* **113**(26), 263601 (2014).
- ¹⁶M. E. Trusheim, B. Pingault, N. H. Wan, M. Gündoğan, L. De Santis, R. Debroux, D. Gangloff, C. Purser, K. C. Chen, M. Walsh, J. J. Rose, J. N. Becker, B. Lienhard, E. Bersin, I. Paradeisanos, G. Wang, D. Lyzwa, A. R.-P. Montblanch, G. Malladi, H. Bakhrü, A. C. Ferrari, I. A. Walmsley, M. Atatüre, and D. Englund, "Transform-limited photons from a coherent tin-vacancy spin in diamond," *Phys. Rev. Lett.* **124**(2), 023602 (2020).
- ¹⁷P. Siyushev, M. H. Metsch, A. Ijaz, J. M. Binder, M. K. Bhaskar, D. D. Sukachev, A. Sipahigil, R. E. Evans, C. T. Nguyen, M. D. Lukin, P. R. Hemmer, Y. N. Palyanov, I. N. Kupriyanov, Y. M. Borzdov, L. J. Rogers, and F. Jelezko, "Optical and microwave control of germanium-vacancy center spins in diamond," *Phys. Rev. B* **96**(8), 081201 (2017).
- ¹⁸J. E. Fröch, A. Bahm, M. Kianinia, Z. Mu, V. Bhatia, S. Kim, J. M. Cairney, W. Gao, C. Bradac, I. Aharonovich, and M. Toth, "Versatile direct-writing of dopants in a solid state host through recoil implantation," *Nat. Commun.* **11**(1), 5039 (2020).
- ¹⁹L. Rondin, J.-P. Tetienne, T. Hingant, J.-F. Roch, P. Maletinsky, and V. Jacques, "Magnetometry with nitrogen-vacancy defects in diamond," *Rep. Prog. Phys.* **77**(5), 056503 (2014).
- ²⁰E. Janitz, M. K. Bhaskar, and L. Childress, "Cavity quantum electrodynamics with color centers in diamond," *Optica* **7**(10), 1232–1252 (2020).
- ²¹T. B. Hoang, G. M. Akselrod, C. Argyropoulos, J. Huang, D. R. Smith, and M. H. Mikkelsen, "Ultrafast spontaneous emission source using plasmonic nanoantennas," *Nat. Commun.* **6**(1), 7788 (2015).
- ²²J. Martin, R. Wannemacher, J. Teichert, L. Bischoff, and B. Köhler, "Generation and detection of fluorescent color centers in diamond with submicron resolution," *Appl. Phys. Lett.* **75**(20), 3096–3098 (1999).
- ²³J. Koike, D. M. Parkin, and T. E. Mitchell, "Displacement threshold energy for type IIa diamond," *Appl. Phys. Lett.* **60**(12), 1450–1452 (1992).
- ²⁴J. M. Smith, S. A. Meynell, A. C. Bleszynski Jayich, and J. Meijer, "Colour centre generation in diamond for quantum technologies," *Nanophotonics* **8**(11), 1889–1906 (2019).
- ²⁵J. Meijer, B. Burchard, M. Domhan, C. Wittmann, T. Gaebel, I. Popa, F. Jelezko, and J. Wrachtrup, "Generation of single color centers by focused nitrogen implantation," *Appl. Phys. Lett.* **87**(26), 261909 (2005).
- ²⁶T. Schröder, M. E. Trusheim, M. Walsh, L. Li, J. Zheng, M. Schukraft, A. Sipahigil, R. E. Evans, D. D. Sukachev, C. T. Nguyen, J. L. Pacheco, R. M. Camacho, E. S. Bielejec, M. D. Lukin, and D. Englund, "Scalable focused ion beam creation of nearly lifetime-limited single quantum emitters in diamond nanostructures," *Nat. Commun.* **8**(1), 15376 (2017).
- ²⁷S. Pezzagna, D. Rogalla, H.-W. Becker, I. Jakobi, F. Dolde, B. Naydenov, J. Wrachtrup, F. Jelezko, C. Trautmann, and J. Meijer, "Creation of colour centres in diamond by collimated ion-implantation through nano-channels in mica," *Phys. Status Solidi A* **208**(9), 2017–2022 (2011).
- ²⁸S. Lagomarsino, A. M. Flatae, H. Kambalathmana, F. Sledz, L. Hunold, N. Soltani, P. Reuschel, S. Sciortino, N. Gelli, M. Massi, C. Czelusniak, L. Giuntini, and M. Agio, "Creation of silicon-vacancy color centers in diamond by ion implantation," *Front. Phys.* **8**, 601362 (2021).
- ²⁹The center for production of single-photon emitters at the electrostatic-deflector line of the Tandem accelerator of LABEC (Florence)—Elsevier Enhanced Reader.
- ³⁰U. F. S. D'Haenens-Johansson, A. M. Edmonds, B. L. Green, M. E. Newton, G. Davies, P. M. Martineau, R. U. A. Khan, and D. J. Twitchen, "Optical properties of the neutral silicon split-vacancy center in diamond," *Phys. Rev. B* **84**(24), 245208 (2011).
- ³¹J. O. Orwa, K. Ganesan, J. Newnham, C. Santori, P. Barclay, K. M. C. Fu, R. G. Beausoleil, I. Aharonovich, B. A. Fairchild, P. Olivero, A. D. Greentree, and S. Praver, "An upper limit on the lateral vacancy diffusion length in diamond," *Diamond Relat. Mater.* **24**, 6–10 (2012).
- ³²S. Chakravarthi, C. Pederson, Z. Kazi, A. Ivanov, and K.-M. C. Fu, "Impact of surface and laser-induced noise on the spectral stability of implanted nitrogen-vacancy centers in diamond," *Phys. Rev. B* **104**(8), 085425 (2021).
- ³³D. M. Toyli, C. D. Weis, G. D. Fuchs, T. Schenkel, and D. D. Awschalom, "Chip-scale nanofabrication of single spins and spin arrays in diamond," *Nano Lett.* **10**(8), 3168–3172 (2010).
- ³⁴I. Bayn, E. H. Chen, M. E. Trusheim, L. Li, T. Schröder, O. Gaathon, M. Lu, A. Stein, M. Liu, K. Kisslinger, H. Clevenson, and D. Englund, "Generation of ensembles of individually resolvable nitrogen vacancies using nanometer-scale apertures in ultrahigh-aspect ratio planar implantation masks," *Nano Lett.* **15**(3), 1751–1758 (2015).
- ³⁵K. Ito, H. Saito, K. Sasaki, H. Watanabe, T. Teraji, K. M. Itoh, and E. Abe, "Nitrogen-vacancy centers created by N⁺ ion implantation through screening SiO₂ layers on diamond," *Appl. Phys. Lett.* **110**(21), 213105 (2017).
- ³⁶J. L. Pacheco, M. Singh, D. L. Perry, J. R. Wendt, G. Ten Eyck, R. P. Manginell, T. Pluym, D. R. Luhman, M. P. Lilly, M. S. Carroll, and E. Bielejec, "Ion implantation for deterministic single atom devices," *Rev. Sci. Instrum.* **88**(12), 123301 (2017).
- ³⁷B. K. Ofori-Okai, S. Pezzagna, K. Chang, M. Loretz, R. Schirhagl, Y. Tao, B. A. Moores, K. Groot-Berning, J. Meijer, and C. L. Degen, "Spin properties of very shallow nitrogen vacancy defects in diamond," *Phys. Rev. B* **86**(8), 081406 (2012).
- ³⁸S. Sangtaweesin, B. L. Dwyer, S. Srinivasan, J. J. Allred, L. V. H. Rodgers, K. De Greve, A. Stacey, N. Dontschuk, K. M. O'Donnell, D. Hu, D. A. Evans, C. Jaye, D. A. Fischer, M. L. Markham, D. J. Twitchen, H. Park, M. D. Lukin, and N. P. De Leon, "Origins of diamond surface noise probed by correlating single-spin measurements with surface spectroscopy," *Phys. Rev. X* **9**(3), 031052 (2019).
- ³⁹H. J. Mamin, M. Kim, M. H. Sherwood, C. T. Rettner, K. Ohno, D. D. Awschalom, and D. Rugar, "Nanoscale nuclear magnetic resonance with a nitrogen-vacancy spin sensor," *Science* **339**(6119), 557–560 (2013).
- ⁴⁰T. Staudacher, F. Shi, S. Pezzagna, J. Meijer, J. Du, C. A. Meriles, F. Reinhard, and J. Wrachtrup, "Nuclear magnetic resonance spectroscopy on a (5-nanometer)³ Sample Volume," *Science* **339**(6119), 561–563 (2013).
- ⁴¹L. M. Pham, S. J. DeVience, F. Casola, I. Lovchinsky, A. O. Sushkov, E. Bersin, J. Lee, E. Urbach, P. Cappellaro, H. Park, A. Yacoby, M. Lukin, and R. L. Walsworth, "NMR technique for determining the depth of shallow nitrogen-vacancy centers in diamond," *Phys. Rev. B* **93**(4), 045425 (2016).
- ⁴²K. Ohno, F. Joseph Heremans, L. C. Bassett, B. A. Myers, D. M. Toyli, A. C. Bleszynski Jayich, C. J. Palmstrom, and D. D. Awschalom, "Engineering shallow spins in diamond with nitrogen delta-doping," *Appl. Phys. Lett.* **101**(8), 082413 (2012).
- ⁴³C. Bradac, W. Gao, J. Forneris, M. E. Trusheim, and I. Aharonovich, "Quantum nanophotonics with group IV defects in diamond," *Nat. Commun.* **10**(1), 5625 (2019).
- ⁴⁴A. Gale, J. E. Fröch, M. Kianinia, J. Bishop, I. Aharonovich, and M. Toth, "Recoil implantation using gas-phase precursor molecules," *Nanoscale* **13**(20), 9322–9327 (2021).
- ⁴⁵G. Fischer, G. Carter, and R. Webb, "Recoil implantation from a thick film source," *Radiat. Eff.* **38**(1–2), 41–43 (1978).
- ⁴⁶J. P. Gailliard, "Recoil implantation and ion mixing," in *Surface Engineering: Surface Modification of Materials*, NATO ASI Series, edited by R. Kossowsky and S. C. Singhal (Springer Netherlands, Dordrecht, 1984), pp. 32–47.
- ⁴⁷R. Grötzschel, R. Klabes, U. Kreissig, and A. Schmidt, "Recoil implantation from thin surface films on silicon," *Radiat. Eff.* **36**(3–4), 129–134 (1978).
- ⁴⁸K. Paprocki and I. Brylowska, "Recoil implantation of aluminium into silicon," *Radiat. Eff.* **87**(2), 63–68 (1985).
- ⁴⁹K. R. Williams, K. Gupta, and M. Wasilik, "Etch rates for micromachining processing—Part II," *J. Microelectromech. Syst.* **12**(6), 761–778 (2003).
- ⁵⁰K. Iakoubovskii, I. Kiflawi, K. Johnston, A. Collins, G. Davies, and A. Stesmans, "Annealing of vacancies and interstitials in diamond," *Physica B* **340–342**, 67–75 (2003).
- ⁵¹B. L. Green, A. T. Collins, and C. M. Breeding, "Diamond spectroscopy, defect centers, color, and treatments," *Rev. Mineral. Geochem.* **88**(1), 637–688 (2022).
- ⁵²K.-M. C. Fu, C. Santori, P. E. Barclay, and R. G. Beausoleil, "Conversion of neutral nitrogen-vacancy centers to negatively charged nitrogen-vacancy centers through selective oxidation," *Appl. Phys. Lett.* **96**(12), 121907 (2010).

- ⁵³J. F. Ziegler, M. D. Ziegler, and J. P. Biersack, "SRIM—The stopping and range of ions in matter (2010)," *Nucl. Instrum. Methods Phys. Res., Sect. B* **268**(11), 1818–1823 (2010).
- ⁵⁴P. Spinicelli, A. Dréau, L. Rondin, F. Silva, J. Achard, S. Xavier, S. Bansropun, T. Debuisschert, S. Pezzagna, J. Meijer, V. Jacques, and J.-F. Roch, "Engineered arrays of nitrogen-vacancy color centers in diamond based on implantation of CN-molecules through nanoapertures," *New J. Phys.* **13**(2), 025014 (2011).
- ⁵⁵B. Naydenov, V. Richter, J. Beck, M. Steiner, P. Neumann, G. Balasubramanian, J. Achard, F. Jelezko, J. Wrachtrup, and R. Kalish, "Enhanced generation of single optically active spins in diamond by ion implantation," *Appl. Phys. Lett.* **96**(16), 163108 (2010).
- ⁵⁶S. Sangtawesin, T. O. Brundage, Z. J. Atkins, and J. R. Petta, "Highly tunable formation of nitrogen-vacancy centers via ion implantation," *Appl. Phys. Lett.* **105**(6), 063107 (2014).
- ⁵⁷C. Santori, P. E. Barclay, K.-M. C. Fu, and R. G. Beausoleil, "Vertical distribution of nitrogen-vacancy centers in diamond formed by ion implantation and annealing," *Phys. Rev. B* **79**(12), 125313 (2009).
- ⁵⁸A. Gardill, I. Kemeny, M. C. Cambria, Y. Li, H. T. Dinani, A. Norambuena, J. R. Maze, V. Lordi, and S. Kolkowitz, "Probing charge dynamics in diamond with an individual color center," *Nano Lett.* **21**(16), 6960–6966 (2021).
- ⁵⁹R. E. Evans, A. Sipahigil, D. D. Sukachev, A. S. Zibrov, and M. D. Lukin, "Narrow-linewidth homogeneous optical emitters in diamond nanostructures via silicon ion implantation," *Phys. Rev. Appl.* **5**(4), 044010 (2016).
- ⁶⁰J. P. Goss, P. R. Briddon, M. J. Rayson, S. J. Sque, and R. Jones, "Vacancy-impurity complexes and limitations for implantation doping of diamond," *Phys. Rev. B* **72**(3), 035214 (2005).
- ⁶¹L. Orphal-Kobin, K. Unterguggenberger, T. Pregolato, N. Kemf, M. Matalla, R.-S. Unger, I. Ostermay, G. Pieplow, and T. Schröder, "Optically coherent nitrogen-vacancy defect centers in diamond nanostructures," *Phys. Rev. X* **13**(1), 011042 (2023).
- ⁶²A. Dréau, M. Lesik, L. Rondin, P. Spinicelli, O. Arcizet, J.-F. Roch, and V. Jacques, "Avoiding power broadening in optically detected magnetic resonance of single NV defects for enhanced dc magnetic field sensitivity," *Phys. Rev. B* **84**(19), 195204 (2011).